

Primary Charge Separation Routes in the BChl:BPhe Heterodimer Reaction Centers of *Rhodobacter sphaeroides*[†]

Marion E. van Brederode,[‡] Ivo H. M. van Stokkum,[‡] Evaldas Katilius,[‡] Frank van Mourik,[‡] Michael R. Jones,[§] and Rienk van Grondelle^{*,‡}

Faculty of Sciences, Division of Physics and Astronomy, Department of Biophysics and Physics of Complex Systems, Vrije Universiteit and Institute of Molecular Biological Sciences (IMBW), Vrije Universiteit, de Boelelaan 1081, 1081 HV Amsterdam, The Netherlands, and Division of Molecular Biology and Biotechnology, University of Sheffield, Western Bank, Sheffield, S10 2UH, United Kingdom

Received December 10, 1998; Revised Manuscript Received February 16, 1999

ABSTRACT: Energy transfer and the primary charge separation process are studied as a function of excitation wavelength in membrane-bound reaction centers of *Rhodobacter sphaeroides* in which the excitonically coupled bacteriochlorophyll homodimer is converted to a bacteriochlorophyll-bacteriopheophytin heterodimer, denoted D [Bylina, E. J., and Youvan, D. C. (1988) *Proc. Natl. Acad. Sci. U.S.A.* 85, 7226]. In the HM202L heterodimer reaction center, excitation of D using 880 nm excitation light results in a 43 ps decay of the excited heterodimer, D*. The decay of D* results for about 30% in the formation of the charge separated state D⁺Q_A⁻ and for about 70% in a decay directly to the ground state. Upon excitation of the monomeric bacteriochlorophylls using 798 nm excitation light, approximately 60% of the excitation energy is transferred downhill to D, forming D*. Clear evidence is obtained that the other 40% of the excitations results in the formation of D⁺Q_A⁻ via the pathway B_A* → B_A⁺H_A⁻ → D⁺H_A⁻ → D⁺Q_A⁻. In the membrane-bound “reversed” heterodimer reaction center HL173L, the simplest interpretation of the transient absorption spectra following B excitation is that charge separation occurs solely via the slow D*-driven route. However, since a bleach at 812 nm is associated with the spectrum of D* in the HL173L reaction center, it cannot be excluded that a state including B_B is involved in the charge separation process in this complex.

Reaction centers (RCs)¹ of photosynthetic organisms are transmembrane pigment–protein complexes, in which light energy is used to create a charge-separated state between cofactors located on opposite sites of the membrane. Precise information is available about the orientation of the cofactors and the protein surroundings for the RCs of the purple non-sulfur bacteria *Rhodospseudomonas viridis* and *Rhodobacter (Rb.) sphaeroides* (1, 2), and therefore, an attempt can be made to understand the mechanism of these electron-transfer reactions in molecular terms. One way to achieve this is through the study of site-directed mutants, in which pigment–protein interactions have been modulated and/or the pigment composition changed (3–6). The RC of *Rb. sphaeroides* consists of three protein subunits, termed L, M,

and H. Subunits L and M each have five transmembrane α-helices and bind 10 cofactors. These are four bacteriochlorophyll (BChl) molecules, of which two are monomeric (B_A and B_B) and two form an excitonically coupled dimer (P), two bacteriopheophytin (BPhe) molecules (H_A and H_B), two ubiquinone molecules (Q_A and Q_B), a non-heme iron atom, and a carotenoid molecule. Subunit H has one transmembrane α-helix and a large globular domain. The BChl, BPhe, and ubiquinone cofactors are arranged in two membrane-spanning branches around an axis of 2-fold symmetry that runs perpendicular to the plane of the membrane.

Despite the almost 2-fold symmetry in the arrangement of the cofactors and the large homology between the L and M polypeptides, it appears that electron transfer only proceeds via the so-called active A branch of cofactors (the cofactors which are mainly bound by the L subunit). The lowest excited state of the RC is the excited low exciton state of P (P*), and upon excitation of any of the monomeric bacteriochlorins (i.e., B_A, B_B, H_A or H_B), excitation energy is transferred to P within 100–200 fs (fs) to form P* (7–11). Primary charge separation then starts from P*, and the state P⁺H_A⁻ is formed in approximately 3.5 ps following excitation of P. Since the rate of this process is much too rapid to be explained by direct coupling between H_A and P, the intervening monomeric BChl B_A is involved in this process in some way. Mainly upon the basis of time-resolved

[†] M.R.J. acknowledges support from the Biotechnology and Biological Sciences Research Council and the University of Sheffield. M.E.v.B. and F.v.M. are supported by Dutch Foundation for Fundamental Research (NWO) through the foundation for Life and Earth Sciences (ALW).

* To whom correspondence should be addressed. Fax: 31-20-4447999. E-mail: rienk@nat.vu.nl.

[‡] Faculty of Sciences.

[§] Division of Molecular Biology and Biotechnology.

¹ Abbreviations: BChl, bacteriochlorophyll; BPhe, bacteriopheophytin; CT, charge transfer; D, heterodimeric primary electron donor; fwhm, full-width half-maximum; GVD, group velocity dispersion; IRF, instrument response function; P, homodimeric primary electron donor; Q, quinone; QY, quantum yield; *Rb.*, *Rhodobacter*; RC, reaction center; SADS, species associated difference spectrum; WT, wild-type.

absorbance difference measurements around 1020 nm, where B_A^- shows a distinct absorbance band, it is now becoming widely accepted that the state $P^+B_A^-$ is formed as a discrete intermediate in the electron-transfer pathway from P^* to $P^+H_A^-$ (12–14). Analysis of kinetic data in terms of this two-step electron-transfer model results in lifetimes of ~ 3 – 5 ps for the electron-transfer $P^* \rightarrow P^+B_A^-$ and ~ 1 – 2 ps for the electron-transfer $P^+B_A^- \rightarrow P^+H_A^-$. However, not all of the features of P^* driven charge separation are completely understood, and many basic issues are still under debate, such as the fact that the primary charge separation is unidirectional, the role of an internal charge transfer (CT) state in P^* , the presence of coherent nuclear motion on the time scale of electron transfer, the dynamic role of the protein in stabilizing the charge separated products, heterogeneity of the RC population, and the energy levels of the states $P^+B_A^-$ and $P^+H_A^-$ on different time scales (see, for review, refs 3–6).

Recently, the picture of primary events in the RC has become even more complicated with the discovery that the sequence of primary events described above is not the only route by which energy captured by the RC can result in the formation of $P^+H_A^-$ (11, 15–23). These new routes of primary charge separation involve the excited state of B_A (and possibly also H_A) and have been suggested to involve the primary reactions $B_A^* \rightarrow P^+B_A^-$ and $B_A^*/H_A^* \rightarrow B_A^+H_A^-$. These new primary reactions are observed to take place on a subpicosecond time scale, i.e., on a time scale before energy transfer from B_A^* to P has been completed. In particular, RCs with the mutations YM210W and YM210L have been instrumental in the identification of these new charge-transfer routes. At cryogenic temperatures, these RCs perform very slow P^* -driven charge separation and therefore allow the resolution of rapid B_A^* -driven electron transfer which, in the WT RCs, is commensurate with electron-transfer driven by P^* . In the YM210W/L RCs, it was shown that $P^+B_A^-$ and $B_A^+H_A^-$ are formed from B_A^* on a subpicosecond time scale without the involvement of P^* as an intermediate (18, 21). Both states formed from B_A^* subsequently evolved to $P^+H_A^-$ within several picoseconds.

In this work, we have studied the presence of alternative charge separation routes in the BChl-BPhe heterodimer RCs in which one of the BChl molecules that is part of the P dimer is replaced by a BPhe. These changes in the cofactor composition are achieved by replacement of the histidine that ligands to the Mg of the P BChl (either HM202 or HL173) by a nonliganding leucine residue (24). The BChl closest to the active A branch of cofactors is replaced by BPhe in the HM202L mutant, and the BChl closest to the inactive B branch of cofactors is replaced in the HL173L mutant. Crystallographic studies have revealed that in both heterodimer RCs the BPhe part of the heterodimer is oriented similarly as the corresponding P BChl in the WT RC and that the protein surroundings of the special pair in the heterodimer is not significantly altered (25). Both heterodimer RCs perform electron transfer from the excited state of the heterodimer primary donor (denoted D^*) to $D^+H_A^-$ and subsequently to $D^+Q_A^-$ (26), but in both heterodimer RCs, the detailed properties of these processes are changed dramatically. These changes appear to originate largely from the 200–300 mV higher redox-potential of the BPhe half of the heterodimer than of the BChl part (27), of which one

of the consequences is that in the oxidized heterodimer D^+ the plus charge is no longer approximately symmetrically distributed between the two halves of the dimer, but is localized completely on the BChl half (28–32). The difference in redox potential between BChl and BPhe also causes a lowering of the free energy of the internal CT state $D_{BChl}^+D_{BPhe}^-$ and an increase of the free energy of the CT state $D_{BChl}^-D_{BPhe}^+$ compared with the free energy of the more degenerate states $P_A^+P_B^-$ and $P_A^-P_B^+$ in the WT RC. As a result, in both heterodimer mutants the D^* state is more strongly coupled to the lowest internal CT state ($D_{BChl}^+D_{BPhe}^-$) than it is the case for the analogous states in the WT RC. Evidence for this stronger coupling comes from the D^* absorbance difference spectrum around 650 nm where the BPhe anion present in the $D_{BChl}^+D_{BPhe}^-$ state exhibits an absorbance increase (26, 33–38), from Stark absorption measurements (39, 40), from vibrational spectroscopy (32, 38), and from theoretical simulation of the ground-state absorbance and Stark spectrum (41, 46). From a simulation of the optical absorbance spectrum of the HM202L RC, it was suggested that the internal CT state $D_{BChl}^+D_{BPhe}^-$ is approximately degenerate with the lowest D^* exciton state (46). The energy level of this CT state can be modulated by the combination of the HM202L mutation with mutations that add or remove hydrogen bonds to the BChl or BPhe part of D, respectively (30, 38, 46). Despite the opposite direction of the dipole of the CT state that is coupled to D^* in the HM202L RC versus that in the HL173L RC, it was concluded from pump–probe experiments that both RCs perform electron transfer along the A branch only (26). As a consequence of this observation, it was proposed that asymmetry in the charge distribution of D^* (or P^*) is not the major source for the unidirectional electron transfer in the RC. The quantum yield (QY) for charge separation was decreased in both heterodimer RCs to 40% in the HM202L RC and 50% in the HL173L RC at room temperature following Q_x excitation (33). At cryogenic temperature, values of a similar magnitude were reported (33). A variety of factors have been proposed to contribute to these lower QYs, including the faster decay of D^* to the ground state, the slower rate for the primary electron-transfer reaction, and increased thermal repopulation of D^* from the charge separated states (33). The intrinsic lifetime for the primary reaction $D^* \rightarrow D^+H_A^-$ calculated from the observed lifetime and QY has been estimated to be 45 and 80 ps at room temperature and 80 and 180 ps at 77 K for the HM202L and HL173L RCs, respectively (33). For the HM200L *Rb. capsulatus* RC, values of 30 ps at room temperature and 40 ps at 77 K have been reported for the same process (37). This lowering of the primary charge separation rate is at least partly caused by the higher free energy of the state $D^+H_A^-$ that results from the increased midpoint potential of the D/D^+ redox couple and is comparable to the slowing down of charge separation in other mutants that have a high redox potential for the P/P^+ couple (3–6). The D/D^+ redox potential was determined to be 640 mV in the HM202L RC, which is an increase of 140 mV relative to the ~ 500 mV redox potential of the P/P^+ couple in the WT RC (30). The intrinsic lifetime for the decay of D^* directly to the ground state has been estimated to be 30 and 80 ps for the HM202L and HL173L RCs, respectively (33), which is relatively fast compared with the >200 ps lifetime for P^* decay to the

ground state in the WT RC (5). This relatively high internal conversion rate of D^* in the heterodimer RCs has been accounted for by the coupling of the exciton state with the internal CT state, which promotes rapid internal conversion of D^* (33).

In this work, we have studied the two heterodimer RCs to investigate the influence of the charge distribution in the ground and excited state of D on the energy and electron-transfer processes following excitation of B, since in these RCs a different environment has been created for B_A and B_B . In the HM202L RC, B_A is located between two BPhe molecules while, in the HL173L RC, it is located between a BChl and a BPhe; the opposite is the case for B_B . In both mutants, the BChl:BPhe heterodimer has a δ -positive/ δ -negative character in both the ground state (caused by the permanent dipole moment of D) and in the excited state [caused by charge resonance (CR) interaction of D^* with the internal CT state]. These δ^+/δ^- charges on D are expected to influence the energy level of a positive or negative charge on the adjacent B_A BChl and, thus, to affect the free energy of states such as $D^+B_A^-$ and $B_A^+H_A^-$ that participate in B_A^* -driven electron-transfer pathways that have been identified in RCs that contain the BChl homodimer. For membrane-bound HM202L heterodimer RCs, both steady-state and time-resolved experiments were performed in order to study the efficiency of energy transfer and charge separation and the characteristics of the primary electron-transfer reactions following excitation of D and of B. To compare the effect of the charge distribution of D on the processes driven by B^* , pump-probe experiments with excitation of B are described for the membrane-bound HL173L "reverse" heterodimer RCs. To prevent confusion, it should be noted that all previous studies which have investigated the heterodimer RCs with pump-probe spectroscopy involved either direct excitation of D around 870 nm or, in cases where the D region was probed, Q_x excitation around 582 nm (26, 33–38).

MATERIAL AND METHODS

Sample Preparation. Construction of the HL173L and HM202L mutant strains of *Rb. sphaeroides* was achieved by mismatch oligonucleotide-mediated site-directed mutagenesis, using the procedures described in refs 42 and 43. Changes in DNA sequence were confined to codons L173 and M202. In both cases, the mutant RC genes were expressed on a derivative of plasmid pRKEH10D (44) in a strain of *Rb. sphaeroides* strain DD13 that lacks the structural genes for the light harvesting complexes, giving "RC-only" strains (44). Both mutant strains were grown under semi-aerobic conditions in the dark; the preparation of RC-only membranes for spectroscopic measurements was as described in ref 45.

Fluorescence Excitation Spectrum. The 77 K steady-state fluorescence excitation spectrum of the HM202L RC was recorded by scanning a Continuous Wave Ti-Sapphire laser (Coherent), pumped by an Ar-ion laser (Coherent), between 750 and 914 nm. The fluorescence was detected perpendicular to the excitation light magic angle through a 10 nm full-width at half-maximum (fwhm) interference filter centered around 950 nm using a polychromator charge coupled device (CCD) setup (Chromex). Excitation power was

measured with a power meter (Delta Developments), which was calibrated for wavelength sensitivity. Excitation power was 400 μ W on an excitation surface of 1 cm^2 . The optical density of the sample was 0.3 at the wavelength of maximal absorption at 77 K. The fluorescence emission spectrum was measured using the same setup and was corrected for the wavelength sensitivity of the detector.

Action Spectrum of Charge Separation. The efficiency of charge separation (i.e., $D^+Q_A^-$ formation) as a function of excitation wavelength was measured as described in ref 17 by scanning a vertically polarized excitation beam from a Ti-Sapphire laser (see above) between 750 and 910 nm and detecting the absorbance difference at magic angle induced by the excitation beam using a double lock-in technique (46). The integrated bleach of the D absorbance between 850 and 930 nm corrected for the excitation intensity was used as a measure for the relative QY of $D^+Q_A^-$ formation. The excitation power was 400 μ W on an excitation surface of 1 cm^2 .

Time-Resolved Spectroscopy. Transient absorbance difference spectra were recorded at magic angle using a femtosecond laser spectrometer essentially as described in ref 18. The fwhm of the instrument response function (IRF) was 350 fs, corresponding to a pulse width of 200 fs. The spectral bandwidth of the excitation pulse was 10 nm fwhm. Data were collected over a spectral range extending over 130 nm centered at 800 or 900 nm. For each time series, spectra were measured at 91–134 delay times between –0.3 and 90–470 ps. Between 40 and 80 spectra were recorded in the first 5 ps. In each wavelength region, between 1 and 4 time series were recorded. The maximal absorbance of the B absorbance band was typically 0.7, and typically 15% of the RCs were excited per pulse which resulted in a maximal bleach of the D absorbance band of 0.02.

Data Analysis. Global analysis of the data was performed as described in ref 13 and 18, with the addition that the wavelength dependence of time-zero due to group velocity dispersion (GVD) was explicitly taken into account in the analysis procedure. To achieve this, the rise and decay of the optical Kerr signal in CS_2 measured over the different wavelength windows was analyzed simultaneously with a third-order polynomial function to describe the variation of time-zero of the instrument response function (IRF). The parameters of the polynomial function and IRF obtained from the CS_2 data were fixed in the analysis of the pump-probe experiments of the RCs. The datasets measured over the different wavelength regions were scaled such that the overlapping wavelength regions had the same amplitude. The spectra in Figures 2–5 are smoothed averages of the fitted results of the overlapping datasets and are corrected for IRF and GVD. Figures showing parts of the individual measured spectra used for the analysis together with the result of the fit are available as Supporting Information.

RESULTS

HM202L RC: Steady-State Fluorescence Excitation and Action Spectrum for $D^+Q_A^-$ Formation. Figure 1A shows the 77 K fluorescence excitation spectrum and fluorescence emission spectrum of the HM202L RC with Q_A in the neutral state. The fluorescence excitation spectrum is compared with the one minus transmission spectrum, and the two spectra

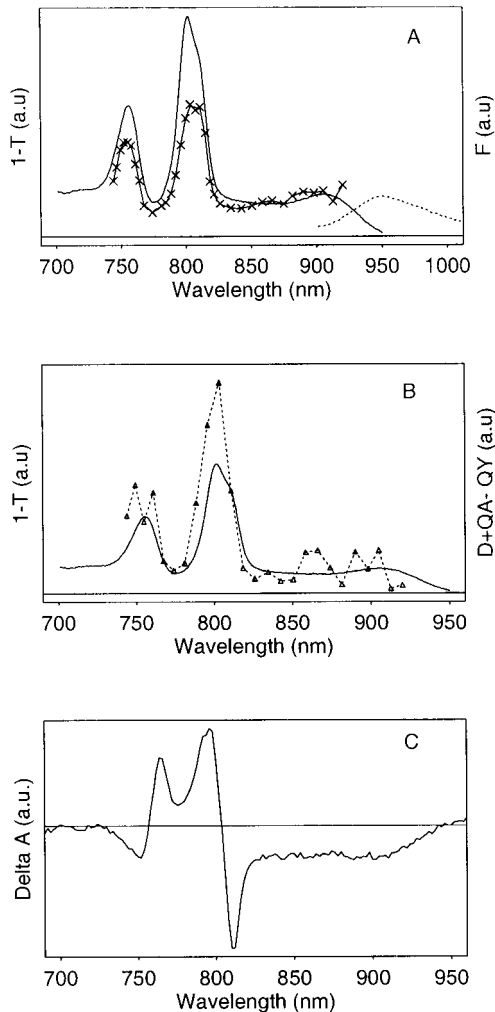


FIGURE 1: (A) Excitation spectrum of fluorescence detected at 950 nm (crosses) and 1-T spectrum (solid) of membrane-bound HM202L RCs of *Rb. sphaeroides* at 77 K with Q_A neutral. The fluorescence emission spectrum of the RC, corrected for the wavelength sensitivity of the instrument, is depicted with the dotted line. (B) Action spectrum for $D^+Q_A^-$ formation (triangles) and 1-T spectrum at 77 K of membrane-bound HM202L RCs of *Rb. sphaeroides*. (C) $D^+Q_A^-$ minus DQ_A light-induced absorption difference spectrum of membrane-bound HM202L RCs at 77 K as detected upon modulated excitation.

are normalized on the signal of D between 840 and 915 nm. As reported previously for the analogous energy transfer from H^*/B^* to P^* in the YM210W, YM210F, YM210L, and LM160H/FM197H RCs (17, 21), the efficiency of energy transfer for $H^*/B^* \rightarrow D^*$ is significantly less than 100% in the HM202L RC. This efficiency of energy transfer to D^* can be estimated to be $\sim 60\%$ from B^* and $\sim 70\%$ from H^* . In the region around 800 nm, the absorption of B_A and B_B are partly resolved and, as in the WT RC, the shoulder around 811 nm can be attributed to B_B (47). From the shape of the fluorescence excitation spectrum in the B band region, it is apparent that in particular a significant fraction of the excitation energy residing on B_A is not transferred to D, which is fully in line with our original observation on the YM210W RC (17). The complementary experiment, in which the action spectrum for charge separation ($D^+Q_A^-$ formation) was measured, is shown in Figure 1B. This action spectrum is calculated from the amplitude of the bleach of the D absorbance band in the reversible light-induced

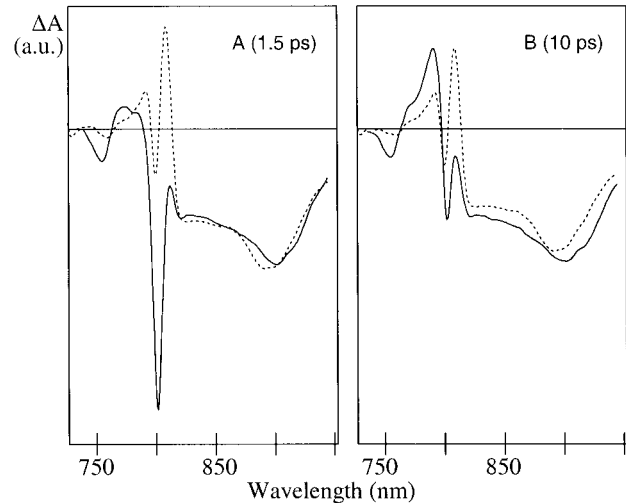


FIGURE 2: Transient absorbance difference spectra of membrane-bound HM202L RCs obtained at 1.5 ps (A) and 10 ps (B) after a ~ 200 fs excitation pulse centered at 798 nm (solid) and 880 nm (dashed). The spectra are reconstructed from the global analysis fit and are corrected for GVD and IRF. The spectra are scaled on the basis of the bleach between 840 and 950 nm at 1.5 ps.

absorbance difference spectrum of $D^+Q_A^-$ (see Figure 1C for a typical spectrum) following excitation at 3–5 nm intervals. The action spectrum in Figure 1B is again compared to the one minus transmission spectrum, with both spectra normalized on the signal of D in the region between 850 and 910 nm. Figure 1B shows that the excitations which were missing in the fluorescence excitation spectrum do give rise to $D^+Q_A^-$ formation, which demonstrates that an alternative route of charge separation is operating in the HM202L RC which does not involve the excited state of the heterodimer, D^* . The action spectrum further reveals that the QY for charge separation is in fact higher following excitation of B and H than upon excitation of D. The surprising conclusion from the data presented in Figure 1, panels A and B, therefore, is that in the HM202L RC the direct path of electron-transfer driven by H_A^* and/or B_A^* is more efficient than the route of charge separation driven by D^* .

HM202L RC: 77K Transient Absorbance Difference Spectra, D versus B Excitation. To characterize the multiple routes of charge separation in the HM202L RC that underlie the data in Figure 1, transient absorbance difference spectra were recorded at 77 K after selective excitation of the D and B absorbance bands. In Figure 2, absorbance difference spectra at a delay time of 1.5 and 10 ps after excitation of D at 880 nm and excitation of B at 798 nm are compared. The spectrum recorded 1.5 ps after excitation of D (Figure 2A, dashed line) shows a bleach of the broad D absorbance band and pronounced features in the region between 780 and 820 nm. This spectrum is attributed to D^* with the bleaching between 850 and 950 nm being due to loss of D ground-state absorbance and the presence of D^* stimulated emission. The band-shift-like features observed in the region between 780 and 820 nm could be interpreted as electrochromic shifts of the B absorbance bands that might be caused by the pronounced charge transfer (CT) character of D^* . The spectrum recorded 10 ps after D excitation (Figure 2B, dashed line) is similar to the spectrum recorded 1.5 ps after D excitation, although the amplitude of the signal has decreased by approximately 15%. This indicates that very

little of D^* has been converted to $D^+H_A^-$ on this time scale and that some D^* has decayed to the ground state.

According to the fluorescence excitation spectrum and action spectrum of $D^+Q_A^-$ formation depicted in Figure 1, panels A and B, excitation at 798 nm results for approximately 60% in energy transfer to D and for about 40% in direct charge separation without the involvement of D^* . In the absorbance difference spectrum obtained 1.5 ps after excitation of B at 798 nm (Figure 2A, solid line), the presence of D^* is observable as a bleach of the broad D absorbance band. However, the pronounced band-shift-like features that characterize D^* in the spectrum obtained after direct excitation of D (Figure 2A, dashed line) are now largely obscured by a strong negative signal at 801 nm, which is consistent with a bleach of the absorbance of the monomeric BChl molecules. In addition to these spectral features in the 800 nm region, a bleach of BPhe absorbance is observed in the difference spectrum at 756 nm. This demonstrates that the fraction of excitations that is not transferred to D, 1.5 ps after excitation, gives rise to a state in which both B and H absorbance bands are bleached, which could very well represent the formation of $B_A^+H_A^-$ (see below). In the spectrum recorded 10 ps after 798 nm excitation (Figure 2B, solid line), the strong bleach of the B absorbance band has evolved into an electrochromic band shift of the B absorbance band, whereas the bleach of the BPhe and D absorbance bands remains. The bleach of the BPhe and D absorbance bands and the strong electrochromic shift of the B absorbance band can be attributed to the presence of $D^+H_A^-$, as for the analogous state $P^+H_A^-$ in WT RCs. However, the spectrum recorded 10 ps after excitation of B must be a mixed state, as it can be concluded from the 880 nm excitation experiment that very little of the D^* formed by energy transfer from B^* will have decayed to $D^+H_A^-$ after only 10 ps. The presence of some contribution from D^* in the spectrum obtained at 10 ps after 798 nm excitation is indicated by the absorbance increase at 808 nm superimposed on the negative red part of the $D^+H_A^-$ band-shift signal (Figure 2B, solid line) which is characteristic for the "pure" D^* spectrum obtained after 880 nm excitation (Figure 2, dashed line).

Summarizing the results depicted in Figures 1 and 2, we conclude that excitation of B using 798 nm excitation results partly in energy transfer to D and partly in a direct charge separation process not involving D^* . Clearly, the two ultrafast processes must be competitive on a femtosecond time scale. After 1.5 ps, this new charge separation process is characterized by a bleach of B and H absorbance, that could be due to the radical pair state $B_A^+H_A^-$ which, at a delay of 10 ps, is converted into a spectrum characteristic for $D^+H_A^-$. For further characterization and verification of this proposal, the result of a global analysis of the full set of transient absorbance difference spectra for both excitation wavelengths is discussed below.

HM202L RC: Global Analysis of the Transient Absorbance Difference Spectra with an Irreversible Sequential Model. In this section, we will describe how the time constants associated with the spectral changes induced by excitation of the HM202L RC at 798 and 880 nm were obtained from a global analysis of the full set of time-resolved difference spectra using an irreversible sequential model. The irreversible sequential model assumes that the time dependence of the light-driven process can be described

by a sequence of exponentially decaying reactions, with increasing lifetimes, i.e., $1 \rightarrow 2 \rightarrow 3 \dots$ with $\tau_1 < \tau_2 < \tau_3 \dots$. In this kinetic model, the first SADS is the product formed by the excitation pulse, the second SADS is formed from the first SADS with a lifetime τ_1 , the third SADS is formed from the second SADS with a lifetime τ_2 , and so on. The last SADS spectrum describes the nondecaying end-spectrum. Since it is not expected that branching or equilibrium reactions take place upon direct excitation of D at 77 K, this irreversible kinetic model is probably close to the true kinetic model for the experiments using 880 nm excitation. This means that these SADS can be attributed to individual species and that the associated lifetimes represent the intrinsic lifetimes of the intermediates. In contrast, excitation at 798 nm of the HM202L RC probably results in a branched reaction, one branch involving charge separation driven directly from B^* , and the second involving energy transfer from B^* to D followed by charge separation from D^* . Consequently, the analysis with the sequential reaction model as described above will result in SADS that represent mixtures of the products of the two parallel pathways.

The SADS resulting from a global analysis of the set of spectra obtained with 880 nm excitation and 798 nm excitation of the HM202L RC are depicted in panels A and B and panels C–F, respectively, in Figure 3. The lifetimes of the SADS are indicated, together with the assignments of the states that contribute to the SADS. The D^* state is formed directly after excitation at 880 nm and is thus represented by the first SADS (Figure 3A). The difference spectrum due to D^* is characterized by a bleach of the broad D absorbance band and by the characteristic pronounced band-shift-like features between 780 and 820 nm discussed above. A lifetime of 43 ps describes the decay of D^* to the end spectrum (Figure 3B). This 43 ps lifetime is in reasonable agreement with the 30 ps lifetime for D^* decay reported by Laporte and co-workers for isolated HM202L RCs at 77 K (33). Comparison of the amplitudes of the bleach of the D ground-state absorbance in the D^* and $D^+Q_A^-$ SADS shows that the 43 ps lifetime describes mainly the decay of D^* to the ground state and that the QY of $D^+Q_A^-$ formation from D^* is approximately 30%. A separate lifetime related to the intermediate formation of $D^+H_A^-$ could not be resolved, which can be accounted for by the fact that $\sim 70\%$ of the decay of D^* is directly to the ground state and that the difference between the $D^+H_A^-$ and $D^+Q_A^-$ spectra is difficult to resolve at very low ΔOD . The low QY of charge separation also causes that the signal-to-noise ratio of the $D^+Q_A^-$ end spectrum is not very high for the 880 nm excitation experiment. The 43 ps lifetime of D^* and the 30% QY of $D^+Q_A^-$ formation result in an intrinsic lifetime of 61 ps for the major process $D^* \rightarrow D$ and of 143 ps for the minor process $D^* \rightarrow (D^+H_A^-) \rightarrow D^+Q_A^-$.

Figure 3, panels C–F, shows the SADS and associated lifetimes arising from the global analysis of the set of difference spectra observed after 798 nm excitation. Excitation of B at 798 nm is partially selective for B_A (47) and thus results in the formation of a B^* state which is a mixture of a major fraction of B_A^* and of a minor fraction of B_B^* . The difference spectrum of B^* formed by the excitation pulse is characterized by a strong negative feature at 802 nm caused by bleach of the ground-state absorbance of the B BChls and stimulated emission from B^* (Figure 3C). The shoulder

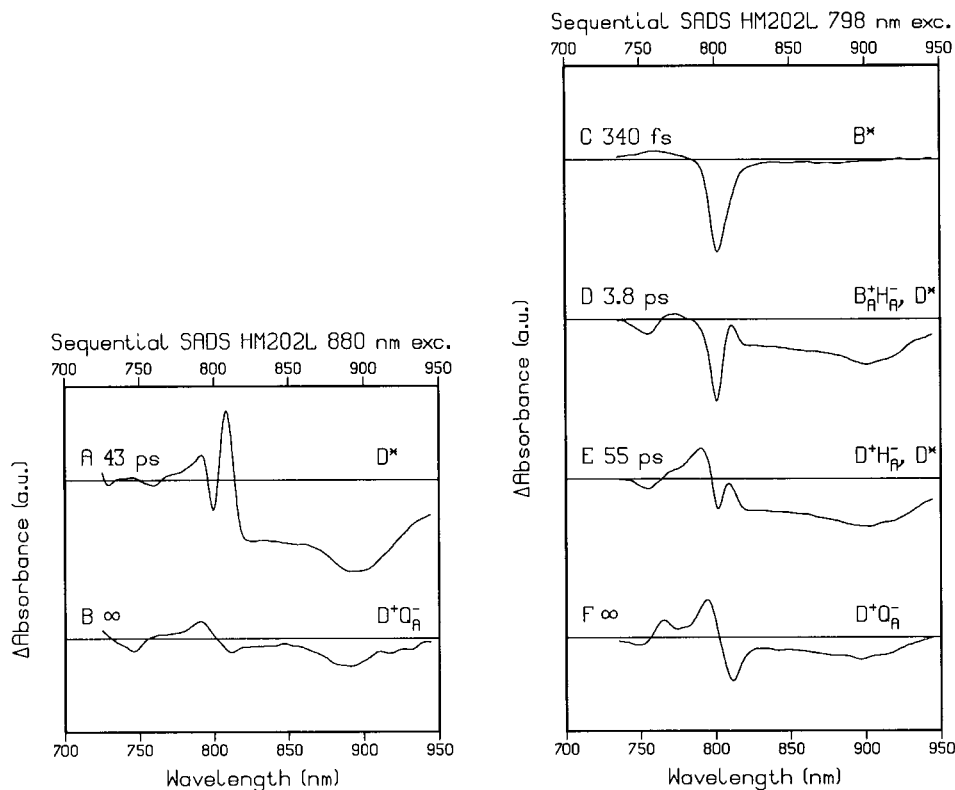


FIGURE 3: SADS and associated lifetimes of membrane-bound HM202L RCs at 77 K derived from a global analysis of the transient absorbance difference spectra obtained after 880 nm (A, B) and 798 nm (C–F) excitation using an irreversible sequential model. For the purpose of comparison, spectrum C has been multiplied by a factor of 0.2.

observed in the ground-state absorbance spectrum around 811 nm, which has been attributed to B_B (47), is not completely bleached in this SADS of B^* . The lifetime associated with the decay of B^* is 340 fs. The SADS of the state(s) that is formed from B^* in 340 fs shows a broad bleach of D absorbance around 900 nm, a strong bleach of B absorbance at 801 nm, and a bleach of BPhe absorbance at 756 nm (Figure 3D). The bleach of D is caused by the formation of D^* following energy transfer from B^* . The band-shift signals in the region between 770 and 820 nm that are also characteristic for the presence of D^* (see Figure 3A) are largely obscured by an intense bleach of the B absorbance that is apparently caused by that fraction of the excited B^* population that has not transferred excitation energy to D. The bleach of B in Figure 3D is narrower and blue-shifted compared to the full B absorbance band and thus seems indicative of a bleach of B_A (47). Since also a bleach of BPhe is observed at 756 nm in the SADS of Figure 3D, the bleach of B and H absorbance is attributed to the formation of $B_A^+H_A^-$ from B_A^* . Other states which could account for a bleach of B_A and BPhe absorbance, such as $H_A^+B_A^-$, are highly unlikely given the unfavorable redox potentials of monomeric BChl reduction and BPhe oxidation for such radical pairs (27). In addition, uphill energy transfer from B^* to form $H_{A,B}^*$ should not be possible since fast uphill energy transfer from an excited state fluorescent around 800 nm to a state absorbing at 760 nm should not be possible, particularly at 77 K. A lifetime of 3.8 ps describes the evolution of the states contributing to the SADS in Figures 3D to a state(s) that has a difference spectrum characterized by a band shift of the B absorbance band and an increased bleaching of D (Figure 3E). The extra bleaching of D plus the formation of the band shift in the 800 nm region

can be explained by the transition $B_A^+H_A^- \rightarrow D^+H_A^-$. The D^* formed by energy transfer from B^* is still present in the SADS of Figure 3E since, as is apparent from the 880 nm excitation experiment, decay of D^* takes place on a much slower time scale. The transition of the mixture of D^* and $D^+H_A^-$ contributing to the SADS of Figure 3E to $D^+Q_A^-$ (Figure 3F) is described by a 55 ps lifetime, similar to the lifetime found in the experiment with 880 nm excitation.

The quantum efficiency of charge separation upon B excitation around 798 nm can be estimated from the maximal bleach of the B^* SADS (Figure 3C) and the bleach of the D absorbance band in the $D^+Q_A^-$ SADS (Figure 3F). The extinction coefficient of the total B absorbance band is approximately 6.5 times higher than that of the D absorbance band (in Figure 1 this ratio is somewhat less because one minus transmission spectra are depicted). Since the individual B molecules do not absorb at the same wavelength, we roughly estimate that each individual B absorbance band has a maximal extinction coefficient that is approximately 4.5 times higher than that of the D absorbance band. Furthermore, if we assume that the stimulated emission that contributes to the B^* SADS has only a small Stokes shift (~ 1 nm), the $\sim 18:1$ ratio between the initial B bleach and the final D bleach converts to a QY of roughly 50%. A similar value is obtained by comparison of the amplitude of the maximal D bleach in the SADS of Figure 3D (which is after the suggested $B_A^+H_A^-$ contribution has converted to $D^+H_A^-$) and the final D bleach in the $D^+Q_A^-$ spectrum. The QY values of approximately 30 and 50% for the 880 and 798 nm pump–probe excitation experiments are in general agreement with the relative QY values as estimated in the action spectrum of $D^+Q_A^-$ formation in Figure 1B.

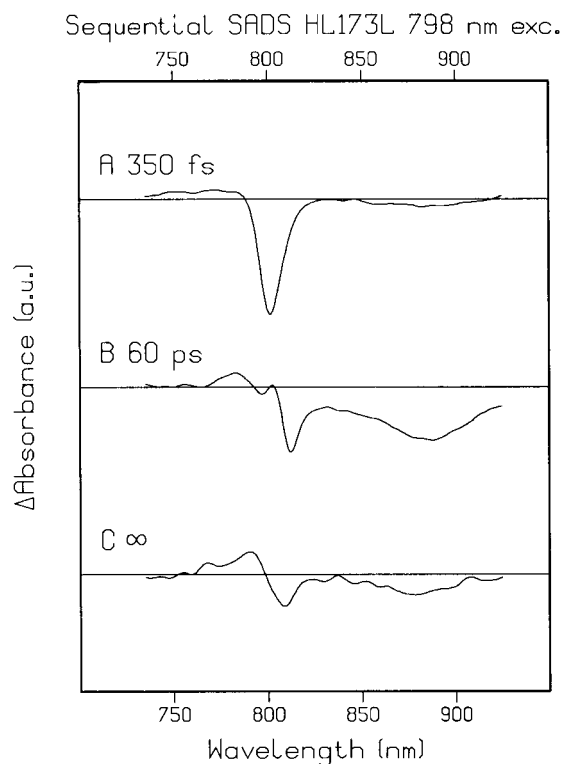


FIGURE 4: SADS and associated lifetimes of membrane-bound HL173L RCs at 77 K derived from a global analysis of the transient absorbance difference spectra obtained after 798 nm excitation using an irreversible sequential model. For the purpose of comparison, spectrum A has been multiplied by a factor of 0.2.

HL173L: Pump-Probe with Excitation of B. To investigate further the effect of an a-symmetric dimer on the electron and energy transfer pathways, pump-probe experiments at 77 K with excitation of B at 798 nm were also performed on the “reversed” heterodimer RC containing the mutation HL173L. The SADS of the HL173L RCs obtained from global analysis using an irreversible sequential model of the dataset are shown in Figure 4, panels A–C. The B^* formed directly after the excitation pulse decays with a lifetime of 350 fs (Figure 4A). The species formed following this decay (Figure 4B) is characterized by a bleach of the broad D absorbance band, a bleach of the red part of the B absorbance band around 812 nm and an absorbance increase between 765 and 790 nm. A lifetime of 60 ps describes the subsequent formation of $D^+Q_A^-$ with a 40% QY (Figure 4C) together with a decay of 60% of D^* directly to the ground state, as can be judged from the decrease in amplitude of the D bleaching signal in the SADS of Figure 4, panels B and C. The 40% QY of $D^+Q_A^-$ formation and the lifetime of 60 ps reported here for membrane-bound HL173L RCs at 77 K with 798 nm excitation is in reasonable agreement with a 40% QY of $D^+Q_A^-$ formation and 100 ps lifetime reported by Laporte and co-workers (33) for detergent isolated HL173L RCs at 77 K with Q_A^- and 880 nm excitation. Also, the spectrum characterizing D^* reported in ref 33 is similar to the spectrum depicted in Figure 4B, exhibiting in particular, a strong bleach of the B band around 810 nm. The interpretation of the different features observed in the spectrum of Figure 4B is however not completely clear. On the one hand, since there is a bleach of D absorbance in Figure 4B and no additional lifetime is observed that could describe the formation of $D^+H_A^-$ via an alternative charge separation

pathway not involving D^* , one could propose that the features observed between 770 and 820 nm in Figure 4B are characteristic for D^* in HL173L RCs. These absorbance changes could represent overlapping electrochromic blue-shift shifts of B_B and B_A induced by the strong CT character of D^* , in which the positive signal of a blue-shift of B_B positioned at 810 nm is overlapped with a negative feature of a blue-shift of B_A positioned at 802 nm (47). In this respect, it should be noted that the D^* state in the HM202L mutant also appears to significantly affect the absorbance properties of the monomeric BChls (see Figure 3A), albeit in a spectroscopically different way. On the other hand, contributions from a bleach of the monomeric BChl pigments to this spectrum cannot be excluded. Since a strong bleach of the red part of the B absorbance is observed in Figure 4B, one could suggest that a state involving B_B , such as $B_B^+H_B^-$, $D^+B_B^-$, or B_B^* , contributes to the “ D^* ” SADS in Figure 4B.

In contrast with the results obtained with the HM202L RC, it is unlikely that a significant amount $B_A^+H_A^-$ contributes to the SADS shown in Figure 4B for the HL173L RC, since the bleach of the B absorbance band peaks at the red edge of the B absorbance band, and there is no clear accompanying bleach of BPhe absorbance (47).

DISCUSSION

HM202L RCs: B^* Driven Charge Separation Investigated by a Target Analysis Using a Branched Kinetic Model. As described in the Results, the steady-state fluorescence excitation spectrum, the action spectrum of $D^+Q_A^-$ formation, and the time evolution of the absorbance difference spectra after 880 and 798 nm excitation of the HM202L RC at 77 K have resulted in a picture for the electron and energy-transfer pathways in this RC. In general agreement with previous reports (see the introductory portion of this article), we observe that excitation of D around 880 nm results in a decay time of 43 ps for D^* that is the result of the formation of the state $D^+H_A^-/D^+Q_A^-$ and decay to the ground state. Upon excitation of B, two pathways are initiated that both start on a subpicosecond time scale, one pathway starts with energy transfer to D and the other with a direct charge separation process. Because the two pathways operate in parallel, the transient absorption difference spectra are at all times the result of the contributions of both pathways. However, it is clear that both pathways operate on different time scales, and therefore, it should in principle be possible to separate both pathways in a so-called target analysis. In a target analysis, the data are fitted directly to a proposed kinetic scheme (13, 53). In principle, the target analysis yields intrinsic rate constants of the transitions and SADS of the individual intermediates, and in this way, it can be tested if the chosen model gives a consistent description of the experimental data. In a complicated model, it is however not possible to determine all the parameters of the transitions independently and it is necessary to use information obtained from other experiments to limit the number of free parameters.

To obtain the intrinsic rate constants and SADS of the true intermediates and to verify the proposed model, a target analysis of the dataset obtained with 798 nm excitation was performed using the branched kinetic model depicted in Figure 5F. Since the model in Figure 5F contains more states and transitions than can be revealed by a completely free fit

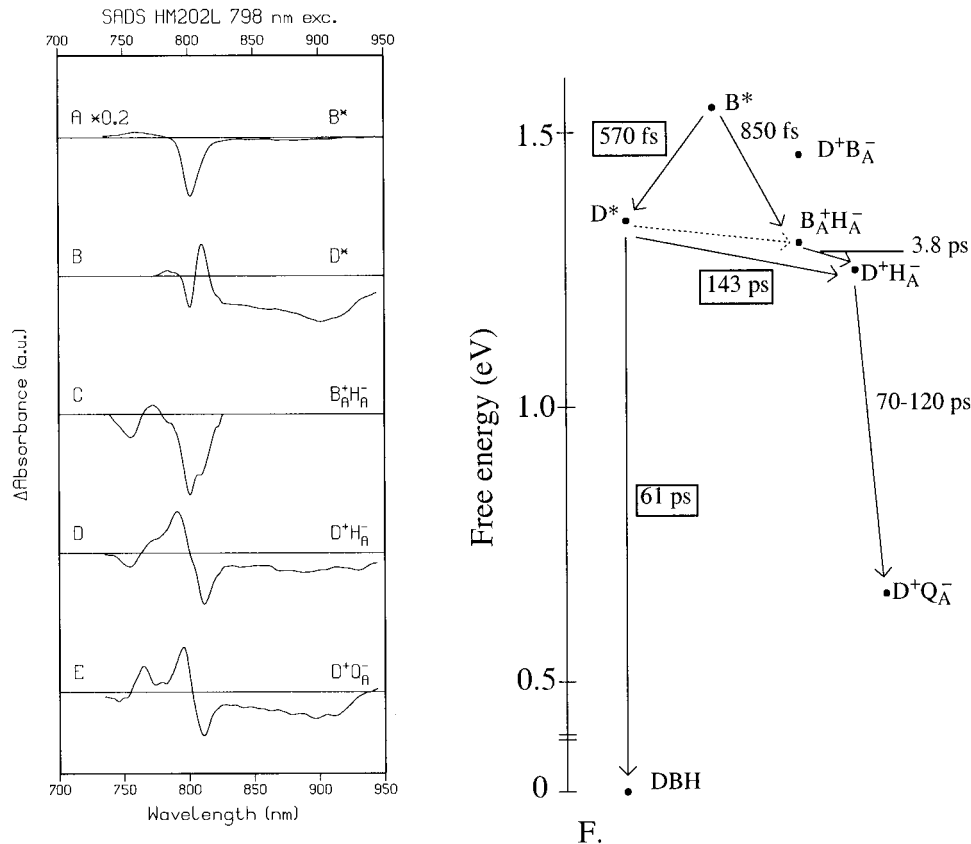


FIGURE 5: (A–E) SADS of the membrane-bound HM202L heterodimer RCs at 77 K derived from a target analysis of the transient absorbance difference spectra obtained after 798 nm excitation using the kinetic scheme depicted in Figure 4F. The assignments of the different SADS to the various states in the scheme are indicated. The intrinsic lifetimes of the various transitions are indicated in Figure 4F. The lifetimes in boxes were fixed parameters in the analysis (see text). For the purpose of comparison, spectrum C has been multiplied by a factor of 0.2.

of the data, the rates of the transitions $B^* \rightarrow D^*$, $D^* \rightarrow D^+H_A^-$, and $D^* \rightarrow D$ were fixed according to information from the other experiments. For the decay of B^* , it is assumed, in accordance with the fluorescence excitation spectrum depicted in Figure 1A, that the 340 fs decay of B^* describes, for 40%, $B^* \rightarrow B_A^+H_A^-$ and, for 60%, $B^* \rightarrow D^*$, which results in a 570 fs lifetime for the energy transfer process $B^* \rightarrow D^*$. To characterize the decay of D^* , the experimental results of the 880 nm excitation experiment were used and the lifetime of the reactions $D^* \rightarrow D^+H_A^-$ and $D^* \rightarrow D$ were fixed to 143 and 61 ps, respectively, which are calculated from the 43 ps lifetime for D^* and the 30% QY for charge separation. Two spectral constraints were also applied to the fit: (i) that the SADS of the intermediate $B_A^+H_A^-$ does not have amplitude above 840 nm and (ii) that the SADS of the intermediate D^* does not have an amplitude in the region between 720 and 770 nm. The latter seems a reasonable approximation of the D^* difference spectrum obtained directly after 880 nm excitation as depicted in Figure 3A. The assumption that the state $B_A^+H_A^-$ does not give rise to a significant signal in the wavelength region above 840 nm is not based on any direct experimental evidence, but seems reasonable, given the broad and flat absorbance spectrum of D, which suggests that any possible electrochromic band shift of D due to the presence of $B_A^+H_A^-$ would not have a large amplitude. It is important to remark that not applying these spectral constraints resulted in SADS with very large standard deviations of the spectral parameters, indicating that at least some spectral constraint was required to limit the number of free fitting parameters

in these wavelength regions. The spectral constraints resulted in only a 0.3% increase of the RMS error of the fit, i.e., from 2.965 to 2.973 mOD.

The SADSs of B^* , D^* , $B_A^+H_A^-$, $D^+H_A^-$, and $D^+Q_A^-$ that result from this target analysis are depicted in Figure 5, curves A–E. The fitted intrinsic rate constants of the transitions that were not fixed in the analysis are depicted without boxes in the kinetic scheme of Figure 5F. The SADS of the five intermediates resulting from the target analysis of the data with the branched kinetic model are consistent with the proposed states. The SADS of B^* (Figure 5A) shows a strong negative feature at 802 nm caused by a bleach of B ground-state absorbance and B^* stimulated emission. The SADS of D^* (Figure 5B) strongly resembles the D^* spectrum as observed after direct excitation of D (Figure 3A), with particularly good agreement between the characteristic band-shift features in the region between 780 and 820 nm. The $B_A^+H_A^-$ intermediate (Figure 5C) shows a bleach of the B and H absorbance bands, and this intermediate is converted with a lifetime of 3.8 ps to $D^+H_A^-$. The $D^+H_A^-$ SADS (Figure 5D) shows a broad bleach of D, an electrochromic band shift of B and a bleach of the BPhe absorbance. There is a small decrease in the apparent amplitude of the H_A bleach between the SADS of $B_A^+H_A^-$ and $D^+H_A^-$. A relatively small amplitude of the H_A bleach in the $D^+H_A^-$ state is a feature that is also observed in the $P^+H_A^-$ spectrum of WT RCs and might be the result of an overlap between the electrochromic band shift of the B absorbance bands and the bleach of H_A . The transition $D^+H_A^- \rightarrow D^+Q_A^-$ is accompanied by a red-shift of the electrochromic bandshift

of the B absorbance band and the development of an electrochromic shift of the H absorbance band (Figure 5E). Also some changes in the shape of the D absorbance bleach are observed between Figure 5, panels D and E. However, we do not consider these changes to be very significant; it is possible that these are the effect of the spectral constraint that the $B_A^+H_A^-$ intermediate does not have an amplitude above 840 nm. The fitted lifetime for the transition $D^+H_A^- \rightarrow D^+Q_A^-$ is strongly correlated with the fixed lifetime for the decay of D^* and was estimated to be between 70 and 120 ps. The most interesting outcome of the target analysis is the resolution of the D^* and $B_A^+H_A^-$ components following B excitation, as this is something that is difficult to achieve in any other way. The fact that a D^* spectrum can be resolved, which in all its major features resembles the D^* spectrum formed after direct excitation at 880 nm, from the target analysis of the data-set obtained with 798 nm excitation is a strong indication that the proposed parallel pathways do occur in the way that is depicted in Figure 5F.

An estimation of the free-energy levels of the various intermediates based on information from the literature and the experiments described has also been indicated in Figure 5F. For D^* the zero-zero transition can be estimated from its red shifted fluorescence spectrum to be located at slightly lower energy than that of P^* in WT RCs, i.e., ~ 925 nm or 1.34 meV. The energy level of B^* (using 798 nm excitation) is estimated to be at the position of maximum bleach assuming a small Stokes shift, i.e., at 802 nm or 1.54 eV. We have not obtained an indication for the involvement of the intermediate $D^+B_A^-$ in any of the electron-transfer pathways operating in the HM202L RC. However, the energy level of this state can be approximated according to the estimated 50 meV energy difference between P^* and $P^+B_A^-$ in WT RCs (52) and the 140 mV increase of the potential of the D/D^+ redox-couple compared with that of the P/P^+ redox-couple in WT RCs (30). This rough calculation places the free-energy level of $D^+B_A^-$ close to that of B^* . This decrease in the free-energy gap between B^* and $D^+B_A^-$ could slow the reaction $B_A^* \rightarrow D^+B_A^-$ and thus explain why this reaction cannot compete with energy transfer and the reaction $B^* \rightarrow B_A^+H_A^-$ on a subpicosecond time scale in the HM202L RC.

On the basis of molecular orbital calculations, the free-energy level of $B_A^+H_A^-$ has been estimated to be either isoenergetic with or below that of P^* in WT RCs (49, 50). The permanent dipole moment present in the ground state of D in HM202L RCs, raises the possibility that the δ^- charge on the D_{BPh_e} adjacent to the oxidized B_A could stabilize the state $B_A^+H_A^-$, and so one might expect that the free-energy level of $B_A^+H_A^-$ is stabilized in the HM202L RC. According to this hypothesis the energy level of $B_A^+H_A^-$ must be placed somewhat below that of D^* in the scheme of Figure 5F. The energy levels of $D^+H_A^-$ and of $D^+Q_A^-$ are estimated according to the estimated free-energy levels of (relaxed) $P^+H_A^-$ and $P^+Q_A^-$ in the WT RC (5) and the 140 mV increase of the potential of the D/D^+ redox couple in the HM202L RC (30).

As described above, the intrinsic lifetimes for $B^* \rightarrow D^*$ energy transfer and $B^* \rightarrow B_A^+H_A^-$ electron transfer are 570 and 850 fs, respectively, in Figure 5F in order to fit both the 340 fs decay of B^* and the 60% efficiency of energy transfer from B^* to D^* upon excitation at 798 nm. Recently, King

and co-workers measured the rise of D^* fluorescence in Q_A reduced HM202L RCs at 80 K following excitation at several wavelengths in the H and B absorption bands (51). They observed that this rise time was biexponential and could be described by lifetimes of 110 and 840 fs for energy transfer from B^* to D^* . From the wavelength dependence of the amplitude of both components, it was concluded that the 840 fs lifetime was associated with the energy transfer reaction $B_A^* \rightarrow D^*$, whereas the 110 fs lifetime described the energy transfer process $B_B^* \rightarrow D^*$. Upon Q_A reduction $B_A^+H_A^-$ might be significantly destabilized, because of the repulsion between Q_A^- and H_A^- . In that case, it is possible that the process $B^* \rightarrow B_A^+H_A^-$ no longer occurs in Q_A reduced HM202L RCs. In this context, it should be noted that, in YM210W RCs, which also perform charge separation partly via the formation of $B_A^+H_A^-$, it has been observed that the pathway $B^* \rightarrow B_A^+H_A^-$ is abolished upon reduction of Q_A , whereas the pathway $B^* \rightarrow P^+B_A^-$ still operates (MEvB et al., unpublished observation). Therefore, it is possible that King and co-workers were in fact looking at a pure energy transfer process in Q_A reduced HM202L RCs, which resulted in a rise time of D^* fluorescence that is in reasonable agreement with the 570 fs lifetime that we attribute to energy transfer in our studies.

According to the kinetic scheme of Figure 5F the intrinsic rate for electron transfer from D^* to $D^+H_A^-$ at 77 K is about $(140 \text{ ps})^{-1}$. Although, this charge separation process driven by D^* is about 2 orders of magnitude slower than charge separation driven by P^* in WT RCs, it is probably still too fast to be explained by a direct coupling between D^* and $D^+H_A^-$. Since a mechanism in which $D^+B_A^-$ is involved as a true intermediate appears to be energetically unfavorable, one could consider the involvement of the intermediate $B_A^+H_A^-$ in D^* -driven charge separation. Such a mechanism has been suggested for WT RCs on the basis of molecular orbital calculations whereby the probability of this mechanism taking place was dependent on the amount of B^* that could mix with P^* (49, 50). The proposed transition from D^* to $B_A^+H_A^-$ in the HM202L RCs is indicated with a dotted line in the kinetic model depicted in Figure 5F. Experimentally, it will be very difficult to verify if this transition takes place, since a slow 30–50 ps population of $B_A^+H_A^-$ (with a 30% QY) from D^* followed by a fast 3.8 ps conversion of $B_A^+H_A^-$ to $D^+H_A^-$ would lead to a very low population of the transient state $B_A^+H_A^-$. In the target analysis, no significant difference in the outcome of the results could be observed between an analysis using a kinetic scheme in which $D^+H_A^-$ was formed directly from D^* or via the intermediate $B_A^+H_A^-$. However, arguments in favor of the proposal that the mechanism involving the reaction $D^* \rightarrow B_A^+H_A^-$ (whereby some B_A^* should be coupled to D^*) does operate in the HM202L RCs are that the 798 nm B excitation experiment showed that $B_A^+H_A^-$ could be populated on a subpicosecond time scale from B_A^* , that $B_A^+H_A^-$ formed from B_A^* could convert to $D^+H_A^-$ with a 3.8 ps lifetime, and that the mechanism which is currently accepted to describe primary charge separation in WT RCs in which $P^+B_A^-$ is involved as a true intermediate is expected to be energetically not possible in the HM202L RC. In line with this proposal it may also be possible that a mechanism involving the formation of $B_A^+H_A^-$ from P^* also operates in mutant RCs in which the P/P^+ redox potential has been

greatly increased, but which still perform a relatively fast P*-driven primary charge separation (48).

CONCLUDING REMARKS

In this work we show that at least two different pathways for electron transfer operate in HM202L heterodimer RCs of *Rb. sphaeroides*. The pathway driven by D* is slow and inefficient due to a fast internal conversion from D* to the ground state, while the alternative pathway, which is selectively driven by B_A* is sufficiently fast to compete effectively with energy transfer from B_A* to D and results in efficient charge separation. The time evolution of the transient spectra clearly identifies B_A⁺H_A⁻ as the first charge separated state following B_A excitation, which is converted to D⁺H_A⁻ on a time scale of 4 ps. The operation of the "new" path makes HM202L RCs more efficient in charge separation following B_A or H_A excitation than following D excitation. The success of the new path is clearly tuned by the properties of the "special pair" dimer as manifested by the absence of the formation of B_A⁺H_A⁻ upon 798 nm excitation of the reverse heterodimer RC HL173L. To explain a decrease in accessibility of B_A⁺H_A⁻ in the HL173L heterodimer RC, it can be argued that the direction of the permanent dipole moment in D, in which the δ-positive charge is now at the position most adjacent to B_A could destabilize the energy level of B_A⁺H_A⁻. These results demonstrate that in general in photosynthetic RCs with a weakened special pair, such as the Photosystem 2 RC of higher plants (54, 55), efficient electron transfer may be initiated by the monomeric pigments in the active branch, provided that certain thermodynamic conditions are fulfilled.

REFERENCES

- Ermiler, U., Fritsch, G., Buchanan, S. K., and Michel, H. (1994) *Structure* 2, 925–936.
- Allen, J. P., Feher, G., Yeates, Y. O., Komiyama, H., and Rees, D. C. (1987) *Proc. Natl. Acad. Sci. U.S.A.* 84, 5730–5734.
- Takakashi, E., and Wraight, C. A. (1994) *Adv. Mol. Cell Biol.* 10, 197–251.
- Allen, J. P., and Williams, J. C. (1995) *J. Bioenerg. Biomembr.* 27, 275–283.
- Woodbury, N. W., and Allen, J. P. (1995) in *Anoxygenic Photosynthetic Bacteria* (Blankenship, R. E., Madigan, M. T., and Bauer, C. E., Eds.) pp 527–557, Kluwer, Dordrecht, The Netherlands.
- Parson, W. W. (1996) in *Protein Electron Transfer*, (Bendall, D. S., Ed.) pp 125–148, Bios Scientific publishers Ltd, Oxford.
- Stanley, R. J., King, B., and Boxer, S. G. (1996) *J. Phys. Chem.* 100, 12052–12059.
- Jonas, D. M., Lang, M. J., Nagasawa, Y., Joo, Y., and Fleming, G. R. (1996) *J. Phys. Chem.* 100, 12660–12673.
- Wynne, K., Haran, G., Reid, G. D., Moser, C. C., Dutton, P. L., and Hochstrasser, R. M. (1996) *J. Phys. Chem.* 100, 5140–5148.
- Haran, G., Wynne, K., Moser, C. C., Dutton, P. L. and Hochstrasser, R. M. (1996) *J. Phys. Chem.* 100, 5562–5569.
- Vos, M. H., Breton, J., and Martin, J.-L. (1997) *J. Phys. Chem.* 101, 9820–9832.
- Arlt, T., Schmidt, S., Kaiser, W., Lauterwasser, C., Meyer, M., Scheer, H., and Zinth, W. (1993) *Proc. Natl. Acad. Sci. U.S.A.* 90, 11757–11763.
- van Stokkum, I. H. M., Beekman, L. M. P., Jones, M. R., van Brederode, M. E., and van Grondelle, R. (1997) *Biochemistry* 36, 11360–11368.
- Kennis, J. T. M., Shkuropatov, A. Ya., van Stokkum, I. H. M., Gast, P., Hoff, A. J., Shuvalov, V. A., and Aartsma, T. J. (1997) *Biochemistry* 36, 16231–16238.
- van Brederode, M. E., Beekman, L. M. P., Kuciasukas, D., Jones, M. R., van Stokkum, I. H. M. and van Grondelle, R. (1996) in *The Reaction Center of Photosynthetic Bacteria* (Michel-Beyerle, M. E., Ed.) pp 225–237, Springer, Berlin-Heidelberg.
- Lin, S., Taguchi, A. K. W., and Woodbury, N. W. (1996) *J. Phys. Chem.* 100, 17067–17078.
- Van Brederode, M. E., Jones, M. R., and van Grondelle, R. (1997) *Chem. Phys. Lett.* 268, 143–149.
- Van Brederode, M. E., Jones, M. R., van Mourik, F., van Stokkum, I. H. M., and van Grondelle, R. (1997) *Biochemistry* 36, 6855–6861.
- Lin, S., Jackson, J., Taguchi, A. K. W., and Woodbury, N. W. (1998) *J. Phys. Chem.* 102, 4016–4022.
- Groot, M.-L., Yu, J.-Y., Agarwal, R., Norris, J. R., and Fleming, G. R. (1998) *J. Phys. Chem.* 102, 5923–5931.
- Van Brederode, M. E., Ridge, J. P., van Stokkum, I. H. M., van Mourik, F., Jones, M. R., and van Grondelle, R. (1998) *Photosynth. Res.* 55, 141–146.
- Zhou, H., Boxer, S. G. (1998) *J. Phys. Chem.* 102, 9139–9147.
- Van Brederode, M. E., van Mourik, F., van Stokkum, I. H. M., Jones, M. R., and van Grondelle, R. (1999) *Proc. Natl. Acad. Sci. U.S.A.* 96, 2054–2099.
- Bylina, E. J., and Youvan, D. C. (1988) *Proc. Natl. Acad. Sci. U.S.A.* 85, 7226–7230.
- Chirino, A. J., Lous, E. J., Huber, M., Allen, J. P., Schenck, C. C., Paddock, M. L., Feher, G., and Rees, D. C. (1994) *Biochemistry* 33, 4584–4593.
- McDowell, L. M., Gaul, D., Kirmaier, C., Holten, D., and Schenck, C. C. (1991) *Biochemistry* 30, 8315–8322.
- Fajer, J., Brune, D. C., Davis, M. S., Forman, A., and Spaulding, L. D. (1975) *Proc. Natl. Acad. Sci. U.S.A.* 72, 4956–4960.
- Bylina, E. J., Kolaczowski, S. V., Norris, J. R., and Youvan, D. C. (1990) *Biochemistry* 29, 6203–6210.
- Huber, M., Isaacson, R. A., Abresch, E. C., Gaul, D., Schenck, C. C., and Feher, G. (1996) *Biochim. Biophys. Acta* 1273, 108–128.
- Allen, J. P., Artz, K., Lin, X., Williams, J. C., Ivancich, A., Albouy, D., Mattioli, T. A., Fetsch, A., Kuhn, M., and Lubitz, W. (1996) *Biochemistry* 35, 6612–6619.
- Vrieze, J., Schenck, C. C., and Hoff, A. J. (1996) *Biochim. Biophys. Acta* 1276, 229–238.
- Albouy, D., Kuhn, M., Williams, J. C., Allen, J. P., Lubitz, W., and Mattioli, T. A. (1997) *Biochim. Biophys. Acta* 1321, 137–148.
- Laporte, L., McDowell, L. M., Kirmaier, C., Schenck, C. C., and Holten, D. (1993) *Chem. Phys.* 176, 615–629.
- Kirmaier, C., Holten, D., Bylina, E. J., and Youvan, D. C. (1988) *Proc. Natl. Acad. Sci. U.S.A.* 85, 7562–7566.
- Kirmaier, C., Bylina, E. J., Youvan, D. C., and Holten, D. (1989) *Chem. Phys. Lett.* 159, 251–257.
- McDowell, L. M., Kirmaier, C., and Holten, D. (1990) *Biochim. Biophys. Acta* 1020, 239–246.
- McDowell, L. M., Kirmaier, C., and Holten, D. (1991) *J. Phys. Chem.* 95, 3379–3383.
- Laporte, L. L., Palaniappan, V., Davis, D. G., Kirmaier, C., Schenck, C. C., Holten, D., and Bocian, D. F. (1996) *J. Phys. Chem.* 100, 17696–17707.
- DiMaggio, T. J., Bylina, E. J., Angerhofer, A., Youvan, D. C., and Norris, J. R. (1990) *Biochemistry* 29, 899–907.
- Hammes, S. L., Mazzola, L., Boxer, S. G., Gaul, D. F., and Schenck, C. C. (1990) *Proc. Natl. Acad. Sci. U.S.A.* 87, 5682–5686.
- Lathrop, E. J. P., and Friesner, R. A. (1994) *J. Phys. Chem.* 98, 3056–3066.
- Beekman, L. M. P., van Stokkum, I. H. M., Monshouwer, R., Rijnders, A. J., McGlynn, P., Visschers, R. W., Jones, M. R., and van Grondelle R. (1996) *J. Phys. Chem.* 100, 7256–7268.
- Vos, M. H., Jones, M. R., Breton, J., Lambry, J.-C., and Martin, J.-L. (1996) *Biochemistry* 35, 2687–2692.

44. Jones, M. R., Visschers, R. W., van Grondelle, R., and Hunter, C. N. (1992) *Biochemistry* 31, 4458–4465.
45. Jones, M. R., Heer Dawson, M., Mattioli, T. A., Hunter, C. N., and Robert, B. (1994) *FEBS Lett.* 339, 18–24.
46. Kwa, S. L. S., Völker, S., Tilly, N. T., van Grondelle, R., and Dekker, J. P. (1994) *Photochem. Photobiol.* 59, 219–228.
47. Breton, J., Bylina, E. J., and Youvan, C. Y. (1989) *Biochemistry* 28, 6423–6430.
48. Woodbury, N. W., Lin, S., Lin, X., Peloquin, J. M., Taguchi, A. K. W., Williams, J., and Allen, J. P. (1995) *Chem. Phys. Lett.* 197, 405–421.
49. Fischer, S. F., and Scherer, P. O. J. (1987) *Chem. Phys.* 115, 151–158.
50. Creighton, S., Hwang, J.-K., Warshel, A., Parson, W. W., and Norris, J. (1988) *Biochemistry* 27, 774–781.
51. King, B. A., Stanley, R. J., and Boxer, S. G. (1997) *J. Phys. Chem.* 101, 3644–3648.
52. Huber, H., Meyer, M., Nagele, T., Hartl, I., Scheer, H., Zinth, W., and Wachtveitl, J. (1995) *Chem. Phys.* 197, 297–305.
53. Holzwarth, A. R. (1996) in *Biophysical Techniques in Photosynthesis* (Amesz, J., and Hoff, A. J., Eds.) pp 75–92 Kluwer, Dordrecht, The Netherlands.
54. Durrant, J. R., Klug, D. R., Kwa, S. L. S., van Grondelle, R., Porter, G., and Dekker, J. P. (1995) *Proc. Natl. Acad. Sci. U.S.A.* 92, 4798–4804.
55. Peterman E. J. G., van Amerongen H., van Grondelle R., and Dekker J. P. (1997) *Proc. Natl. Acad. Sci. U.S.A.* 95, 6128–6133.

BI9829128

Supporting Material.

Typical datasets of transient absorbance difference spectra of the HM202L RC recorded at 77 K after a 200 fs 798 nm excitation pulse, Figure S1 (detection between 735 and 865 nm), S2 (detection between 825 and 945 nm) and a 200 fs 880 nm excitation pulse, Figure S3 (detection between 725 and 840 nm) and S4 (detection between 815 and 945). The result of the global analysis fit is depicted with the dashed line. For 798 nm excitation only half of the spectra are depicted.

To follow the spectral evolution in time the spectra should be inspected bottom-up. The spectrum bottom left is the first spectrum and is recorded before time zero. The delay interval of the spectra as recorded during the experiment is indicated on the y-axis. These values are somewhat arbitrary and deviate approximately -400 fs (S1), 200 fs (S2), 600 fs (S3) and -140 fs (S4) from the values obtained after correction for the position of time-zero in the analysis later. Note that the temporal behaviour of these spectra at early times are influenced by group velocity dispersion (see Material and Method section).

The insets show the residuals of the fit for each spectrum. Because of lack of space, these residuals are not shown in Figure S3. Note that all the spectra are scaled to their extrema. This figure is delivered as a PDF format and can be easily enlarged by software programs such as acroread.

3

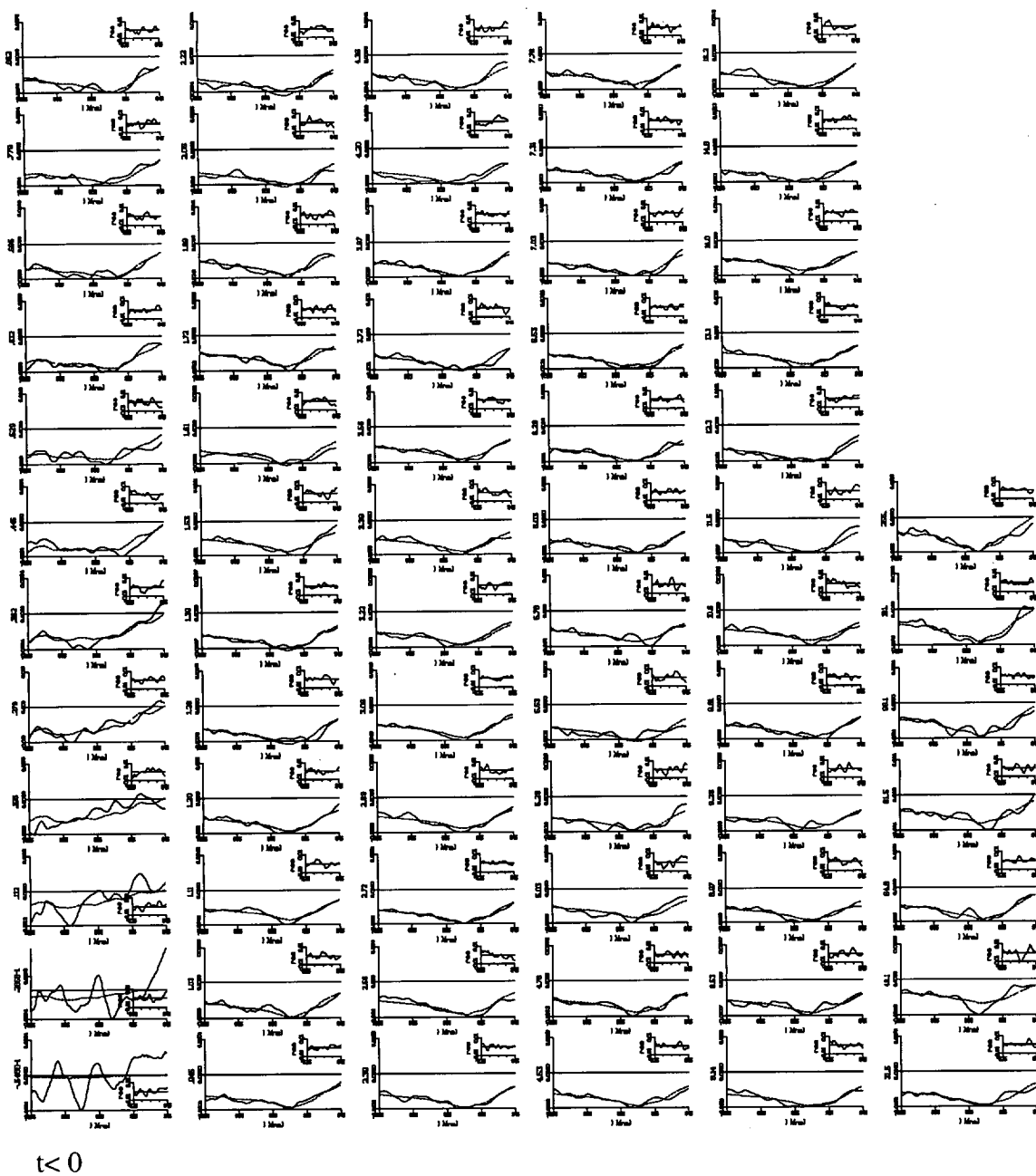


Figure S2.

31

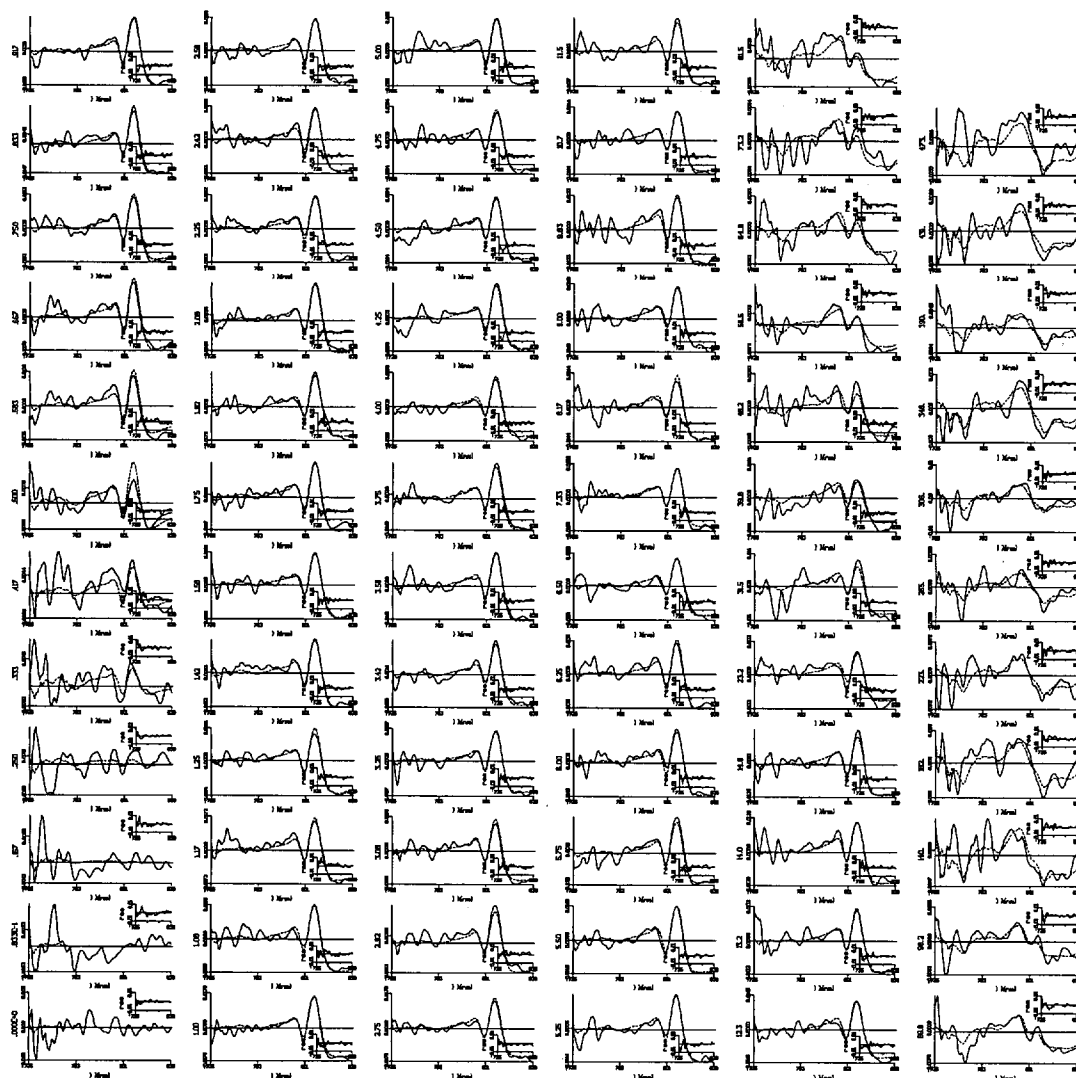


Figure S3.

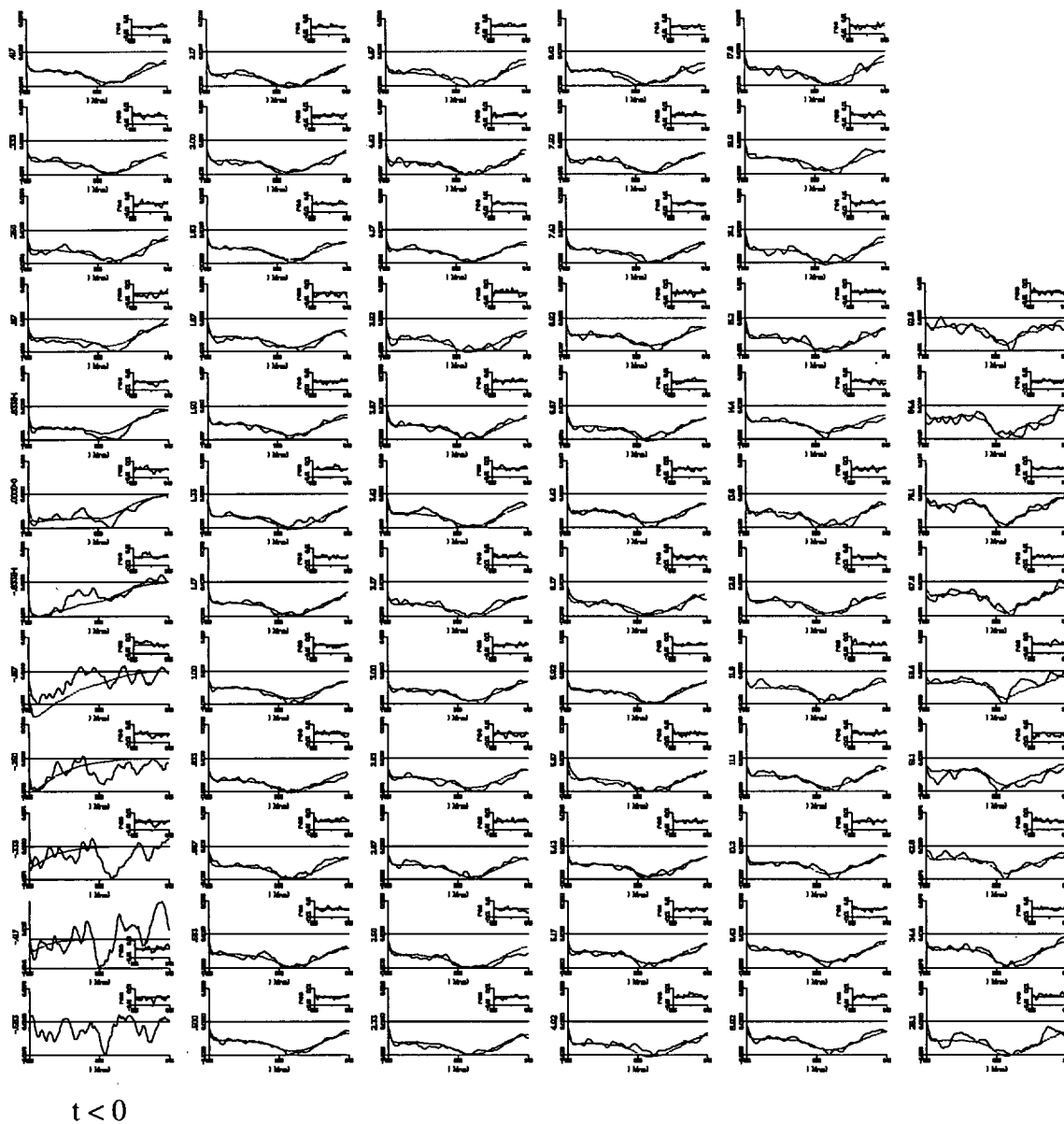


Figure S4.